Physics of Reflective Optics for the Soft Gamma-Ray Photon Energy Range

Mónica Fernández-Perea, Marie-Anne Descalle, Regina Soufli, Klaus P. Ziock, Jennifer Alameda, Sherry L. Baker, Tom J. McCarville, Veijo Honkimäki, Eric Ziegler, Anders C. Jakobsen, Finn E. Christensen, and Michael J. Pivovaroff

Phys. Rev. Lett. **111**, 027404 — Published 12 July 2013

DOI: 10.1103/PhysRevLett.111.027404

Physics of reflective optics for the soft gamma-ray photon energy range

Mónica Fernández-Perea[1] , Marie-Anne Descalle[1], Regina Soufli[1], Klaus P. Ziock[2], Jennifer Alameda[1], Sherry L. Baker[1], Tom J. McCarville[1], Veijo Honkimäki[3], Eric Ziegler[3], Anders C. Jakobsen[4], Finn E. Christensen[4], and Michael J. Pivovaroff[1]

[1] Lawrence Livermore National Laboratory (LLNL), 7000 East Avenue, Livermore, CA 94550, USA
[2] Oak Ridge National Laboratory (ORNL), 1 Bethel Valley Road, Oak Ridge, TN 37831, USA
[3] European Synchrotron Radiation Facility (ESRF), 6 Rue Jules Horowitz, 38043 Grenoble, France
[4] Danish Technical University (DTU)-Space, Elektrovej 327, DK - 2800 Kongens Lyngby, Denmark

Abstract

Traditional multilayer reflective optics that have been used in the past for imaging at x-ray photon energies as high as 200 keV are governed by classical wave phenomena. However, their behavior at higher energies is unknown, because of the increasing effect of incoherent scattering and the disagreement between experimental and theoretical optical properties of materials in the hard x-ray and gamma-ray regimes. Here, we demonstrate that multilayer reflective optics can operate efficiently and according to classical wave physics up to photon energies of at least 384 keV. We also use particle transport simulations to quantitatively determine that incoherent scattering takes place in the mirrors but it does not affect the performance at the Bragg angles of operation. Our results open up new possibilities of reflective optical designs in a spectral range where only diffractive optics (crystals and lenses) and crystal monochromators have been available until now.

Text

In the last decade the use of reflective optics based on multilayer interference coatings has been gradually extended to ever-increasing photon energies up to about 200 keV[1–5]. Reflective optics are advantageous compared to diffractive optics in that they allow greater flux and design flexibility. They can be used to tailor the reflective response of arbitrarily shaped curved substrate elements, thus allowing a variety of optical configurations. Since the operation of multilayer mirrors is enabled by constructive wave interference phenomena, their performance at higher photon energies could be affected by incoherent scattering effects, which become non-negligible in the hard x-ray and gamma-ray regimes. Therefore, the upper energy limit of operation of these devices is currently unknown.

The use of multilayer interference optics at photon energies exceeding ~100 keV presents many extraordinary technical challenges. As photon energy increases, and in order to satisfy the Bragg condition[6] at the largest possible grazing incidence angle, the multilayer period must be reduced. As individual layers become thinner, they ultimately reach the limit of continuous layer formation imposed by their atomic nature. Inherent layer interface imperfections, such as roughness and diffusion, occupy a significant fraction of the layer thickness and can have a deleterious effect on peak reflectance by scattering light outside of the specular direction. Another difficulty arises from the fact that the incidence angle of operation at these energies is ≤0.1 deg. Therefore, deformations of the substrate surface at low spatial frequencies must be extremely small, requiring state of the art substrate fabrication.

Recent experiments[7] suggest the possibility that the refractive index of materials may be greater than unity in the gamma-ray regime. Other authors have found disagreement between

experimentally determined and tabulated optical constants at photon energies of 180 keV and below[4,8]. These unexpected findings reaffirm the need for experimental determination of the optical response of materials, and in particular of multilayer coatings, in the high photon energy regime.

Here, we demonstrate that WC/SiC multilayer coatings with layer periods in the range of 1-2 nm deposited on sufficiently flat and smooth substrates perform as highly efficient mirrors at 384 keV, according to classical wave physics. Monte Carlo particle transport simulations are employed to demonstrate that even though incoherent (Compton) scattering takes place in the mirror, it does not interfere with its operation at this energy. With a peak reflectance of 52.6% at 384 keV at a grazing angle of 0.063 deg, we obtained a 1000-fold increase in performance compared to a single-layer mirror and extended the photon energy range of applicability by ~200 keV above what is currently available. Our results enable the use of reflective optics in soft gamma ray scientific applications such as nuclear and medical physics and astrophysics.

Four WC/SiC multilayers with period thicknesses from 1 to 2 nm were deposited on smooth and flat glass substrates of dimensions $150 \times 150 \times 6.4$ mm^3 manufactured by Hoya Optics™ and Schott Inc™. The multilayer design parameters are shown in Fig. 1(a). Multilayer films were deposited at Lawrence Livermore National Laboratory (LLNL) in a planar DC-magnetron sputtering deposition system[9]. Transmission Electron Microscopy (TEM) images were obtained at Evans Analytical Group (Sunnyvale, California) with a JEOL 2010 TEM instrument equipped with a 1 Mpixel 794 Gatan camera. Cross section specimen preparation was performed with a focused ion beam (FIB) dual-beam system (FEI Strata 400™). Large Angle X Ray Diffraction

(LAXRD) measurements were performed at LLNL with a PANalytical X'Pert PRO MRD^{TM} instrument using a Cu K_α (8,047.8 eV) x-ray source at step size (2θ) of 0.02°.

Reflectance measurements at beamline ID15A of the European Synchrotron Radiation Facility (ESRF) were performed using the high energy micro-diffraction (HEMD) setup in a θ-2θ geometry with vertical plane of incidence. The mirror was centered on an aluminum stand 250 × 250 mm^2 and 15 mm thick. A double crystal, fixed-exit, Laue-Laue monochromator was used for photon energy selection, which was centered at 378.2 keV with a bandwidth of $\Delta E = 9.8$ keV. The crystals were bent to fulfill the Rowland circle geometry. The bandwidth could be narrowed by rotating one of the monochromator crystals. The beam entrance was located 7.3 m from the sample stage, where a W slit 150 mm long with a 7 μm-vertical gap reduced the beam divergence to 0.024 mdeg. The cross-section of the beam at the sample position was rectangular, 2.5 mm in the horizontal direction and 0.011 mm in the vertical direction. The small size in the vertical direction minimized the size of the beam footprint at grazing angles. Alignment procedures were implemented before each measurement to ensure that the top surface of the sample was parallel to the beam, and that the beam was impinging on the center of the sample top surface. Beamline background was characterized through detector scans performed on the direct beam, without a sample. The detector arm included two sets of slits (JJ-Xrays IB-C30, Denmark) each composed of two 10 mm-thick jaws, which are made of 86.8% WC, 12% Co and 1.2% VC+Cr_3C_2. A brass pipe connected the two slits. The 5 mm thick NaI(Tl) detector was enclosed in a thin aluminum and lead housing. The two slits and detector were located at 590, 1320 and 1360 mm from the sample, respectively.

Substrate roughness was 0.05 nm rms at spatial frequencies from 5×10^{-4} to 0.05 nm^{-1} and substrate slope error was ~1 μrad at spatial frequencies from 6.7×10^{-3} to 1 mm^{-1}, as measured

by atomic force microscopy and full-aperture interferometry, respectively. A cross-sectional TEM image of the 1.5 nm-period multilayer is shown in Fig. 1(b). The sharpness/smoothness of the WC-SiC layer interfaces is excellent and was one of the reasons for the selection of the WC/SiC material pair[10]. Fig. 1(c) shows LAXRD measurements. The broad peak at 2θ=37.4 deg is attributed[11] to the fcc β -WC_{1-x} (111) phase ($0.34<x<0.43$) and indicates that the WC layers are nanocrystalline. The absence of SiC peaks indicates that the SiC layers are largely amorphous. The nanocrystalline (WC) - amorphous (SiC) nature of the layers is at least partially responsible for the high quality of the layer interfaces.

Fig. 2 shows reflectance measurements performed at beamline ID15A of ESRF for an incident beam centered at a photon energy of 378.2 keV with a bandwidth ΔE = 9.8 keV. All samples exhibit a 1st order reflectance peak located at an angle consistent with the Bragg equation. The peak reflectance of the multilayer samples with 1.5 and 2 nm periods is 23% and 50%, respectively, more than 1000 times higher than the reflectance that would be achieved by a single layer of WC at the same angles. For the shorter-period multilayers (d = 1.2 and 1.0 nm), which have their 1st order Bragg peaks located at larger incidence angles, lower peak reflectance values of 0.6% and 0.5% were obtained. The lower reflectance values are presumably due to interface effects and/or quasi-discontinuous layers in the multilayer.

Fig. 3 shows the reflectance measurements from the 1.5 nm-period multilayer. By detuning the monochromator, the central photon energy shifted to 384 keV with a bandwidth ΔE = 3.0 keV. With the narrower bandwidth, the reflectance at the 1st order Bragg peak (0.063 deg) was 52.6%, roughly twice as much as in Fig. 2. The 2nd order Bragg peak can also be seen in the figure. The solid line in Fig. 3 shows a calculation performed with the IMD software[12]. IMD employs the wave formalism based on Fresnel equations[14], and has been extensively validated at much lower

photon energies. The multilayer parameters used in the IMD calculations were d = 1.474 nm, Γ_{WC} = 0.43 and σ = 0.275 nm, where d and Γ_{WC} have been defined before and σ is a parameter that combines both the roughness and diffusion at the multilayer interfaces. These parameters were obtained from fits to reflectance measurements performed at 8 and 62 keV, which are discussed elsewhere[15]. The real and imaginary parts of the complex refractive index of WC and SiC were synthesized from the real part of the atomic scattering factors and the total mass attenuation coefficients of W, C and Si, obtained from the literature[16,17]. The mass densities of the WC layers (15.8 g/cm^3) and of the SiC layers (2.98 g/cm^3), obtained from earlier Rutherford backscattering measurements on WC and SiC sputtered thin films[15,18], were also included in the refractive index calculations. In order to account for the incident photon energy bandwidth, IMD reflectance calculations at multiple discrete energies in the bandwidth interval were averaged. The measured and IMD-calculated reflectance values agree at the critical angle and the 1st Bragg peak, indicating that interference phenomena dominate at those angles and suggesting that the optical constants of WC and SiC near 384 keV, calculated using currently available scattering factors and attenuation coefficients[16,17], are accurate. However, there is a background present between the critical angle and the Bragg peaks that cannot be reproduced with the classical wave description.

Given that incoherent (Compton) scattering and other phenomena described below become non-negligible in the gamma ray regime, we attempted to simulate these contributions by using a Monte Carlo particle transport code (MCNP6[13]). Codes such as MCNP are used to model particle transport in complex geometries for photon energies down to 1 keV. The main processes modeled in the code are coherent and incoherent scattering, photoelectric absorption, and pair production. Coherent scattering consists of Rayleigh scattering from the bound electrons (nuclear

Thomson, Delbruck and nuclear resonance scattering are ignored). Incoherent scattering consists of Compton scattering by bound electrons, and takes into account Doppler broadening[19]. The sample model used in the MCNP calculations consisted of two regions, the multilayer treated as a uniform region of homogenized WC and SiC and a fused silica substrate. In the model the photon source was a monoenergetic beam of 378.2 keV photons, since the correction due to the photon energy bandwidth was considered negligible. The 35×35 mm^2 simulated detector tallied the total counts integrated over energy and normalized per source photon. For comparison to experimental data, these values were normalized with the direct beam, obtained by performing the same simulation in absence of a sample. MCNP simulations of the background measurements (without sample) showed that details of the exact shape and composition of the two sets of slits in the detector arm had to be included in order to reproduce the main features observed in the data. MCNP simulations of the reflectance measurements predict that outside of the Bragg peak and the critical angle, over 80% of incident photons scatter in the sample. However, due to the limited solid angle of the slits/detector system, their contribution to the background signal observed in Fig. 3 is negligible. The main background contribution was shown to come from a small portion of the remaining ~20% of photons, which traverse the sample un-collided and then are transmitted through or scattered in the lower blade of the set of slits located closest to the detector. At the Bragg angles and below the critical angle, photons are reflected by the multilayer thin film coating on top of the substrate where most scattering interactions take place, and therefore the optical performance at those angles follows the classical wave theory. If significant scattering occurred in the thin film coating the performance of the mirror would be diminished. The MCNP results are shown in Fig. 3, along with a composite curve calculated assuming that the signals obtained from the particle and wave simulations were additive. The composite curve

shown in Fig. 3 significantly reduces discrepancies between simulation and measurement, raising the overall background while minimally changing the magnitude of the first Bragg peak. The remaining discrepancies are presumably due to the simplified model of the experimental setup and of the scattering processes and data the Monte Carlo code relies upon to model photon transport.

We have demonstrated that multilayer reflective optics can be used to efficiently reflect radiation at photon energies of at least 384 keV. A major implication of this result is the potential use of reflective optics, which allow for higher flux and improved design flexibility, at photon energies where only diffractive elements were available until now. We have shown that outside of the Bragg resonance angles, a large portion (~80%) of the radiation is incoherently scattered by the mirror. Interestingly, scattering is produced across the whole thickness of the mirror (including the substrate) and therefore at the Bragg resonance angles the reflection of photons at the multilayer interfaces takes place before any significant scattering occurs, so the mirror reflective performance remains very high. Our results are consistent with tabulated optical constants, in opposition to what other authors[4,7,8] have found in neighboring photon energy ranges. Habs et al.[7] experimentally determined the real part of the refractive index (δ) of Si at energies from 0.18 to 2 MeV, and found an unexpected sign inversion above 700 keV. Refs. 4 and 8 provided optical constant values for WC and SiC, derived from reflectance measurements on single films in the spectral range from 30 to 180 keV. They found disagreement between their results and tabulated values of the extinction coefficient (k) of SiC. There is no overlap of the photon energies studied here (~384 keV) with the aforementioned photon energy ranges (30-180 keV and > 700 keV), where disagreement with tabulated optical constant values has been reported in the literature. Therefore, our results do not directly contradict the literature. However, additional reflectance

measurements on well-calibrated multilayer coatings such as those presented in this work at photon energies higher and lower than ~380 keV would provide clarity on the behavior of optical constants of materials in the hard x-ray and gamma-ray regime. It is important to note that experimental determinations of optical constants in this regime, where both δ and k are extremely small, are very challenging and can be affected by multiple artifacts such as insufficient substrate flatness, excessive roughness, sample misalignment, and limited incident flux. Today, medical[20,21] and hard x-ray astronomy[22,23] applications in the 20–80 keV range incorporate multilayer mirrors as essential components for highly efficient operation. With our demonstrated high-performance results in the soft gamma-ray band, researchers now have a viable method for realizing instrumentation that can operate at much higher photon energies. Of particular interest are imaging applications that rely on or benefit from detection of discrete emission lines. In nuclear medicine, multilayer mirrors may enhance the resolution of single photon emission computed tomography (SPECT), an imaging technique used in the study of neurological disorders, heart disease and cancer identification[24-26]. While previous researchers designed optics for imaging low-energy lines from a limited number of radionculides[20], with high reflectivity possible up to 400 keV, the most frequently used SPECT radionuclides, including ^{99m}Tc (140 keV), ^{123}I (159 keV), ^{131}I (365 keV), ^{111}In (171 and 245 keV), and ^{201}Tl (167 keV), can now also be used. In astrophysics, soft-gamma ray line emission from radioactive decay[27,28] can be used to probe novae (the 478 keV line from ^{7}Be) and supernovae (the 122 and 136 keV lines from ^{57}Co). More intriguingly, if multilayers can be shown to work at 511 keV, it would be possible to map the location of positron-electron annihilation[29] with unprecedented angular resolution. Such a capability would advance our knowledge of the Galactic sources that produce positrons and could potentially help explain the origin of the

unexplained excess of high-energy positrons recently reported by the Alpha Magnetic Spectrometer (AMS) experiment[30].

Acknowledgements

This work was performed under the auspices of the U.S. Department of Energy by Lawrence Livermore National Laboratory under Contract DE-AC52-07NA27344 and by Oak Ridge National Laboratory, managed by UT-Battelle, under contract DE-AC05-00OR22725. Funding for this research was provided by the National Nuclear Security Administration's Office of Nonproliferation and Verification Research & Development. We acknowledge the European Synchrotron Radiation Facility for provision of synchrotron radiation facilities and the MPI-Stuttgart for access to the High Energy Micro-Diffraction apparatus at ESRF. The contributions of Cynthia Gonsalves and Harry Kawayoshi (Evans Analytical Labs, Sunnyvale, California) in the sample preparation and acquisition of the TEM images is gratefully acknowledged.

a)

d (nm)	N	d_{WC} (nm)	d_{SiC} (nm)	Γ_{WC}
2.0	400	1.0	1.0	0.5
1.5	300	0.6	0.9	0.4
1.2	400	0.6	0.6	0.5
1.0	500	0.45	0.55	0.45

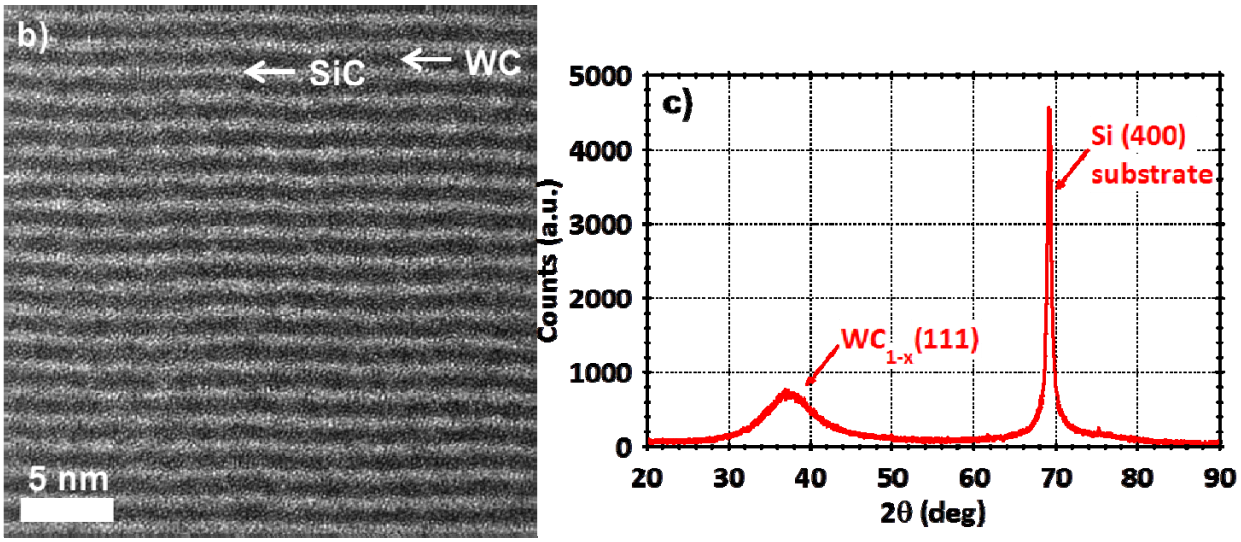

Fig. 1.

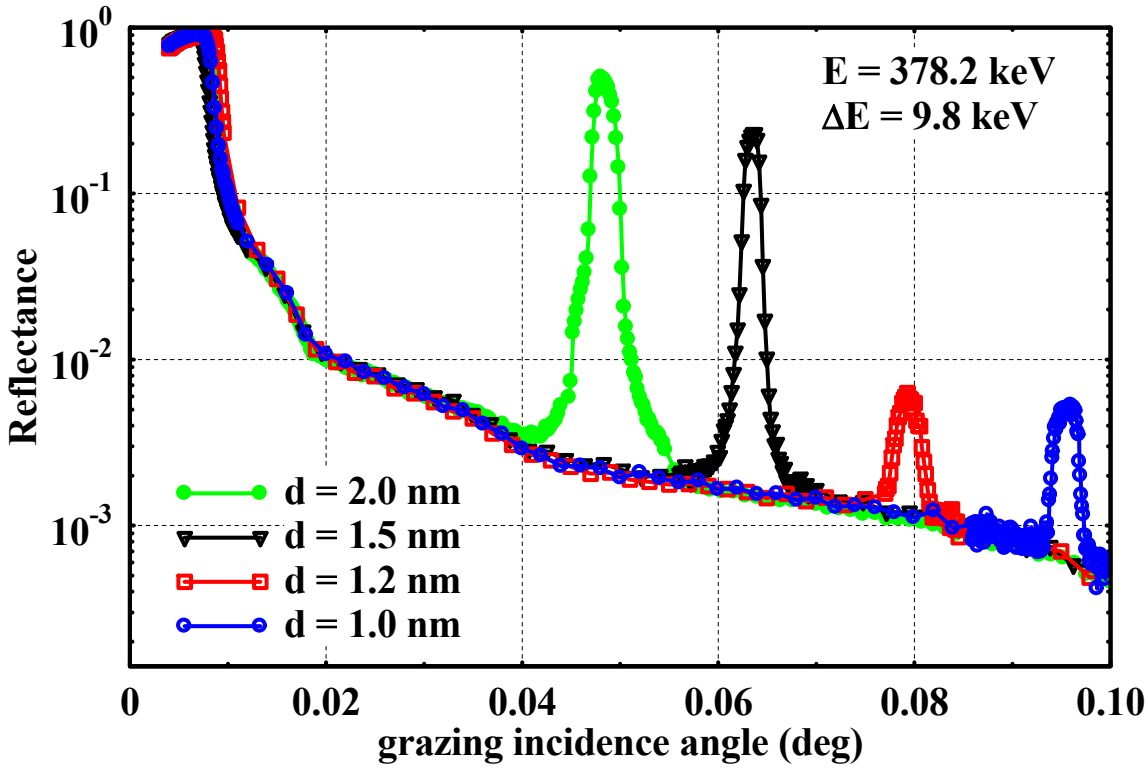
E = 378.2 keV
ΔE = 9.8 keV
d = 2.0 nm
d = 1.5 nm
d = 1.2 nm
d = 1.0 nm
Reflectance
grazing incidence angle (deg)
10^0
10^-1
10^-2
10^-3
0
0.02
0.04
0.06
0.08
0.10

Fig. 2.

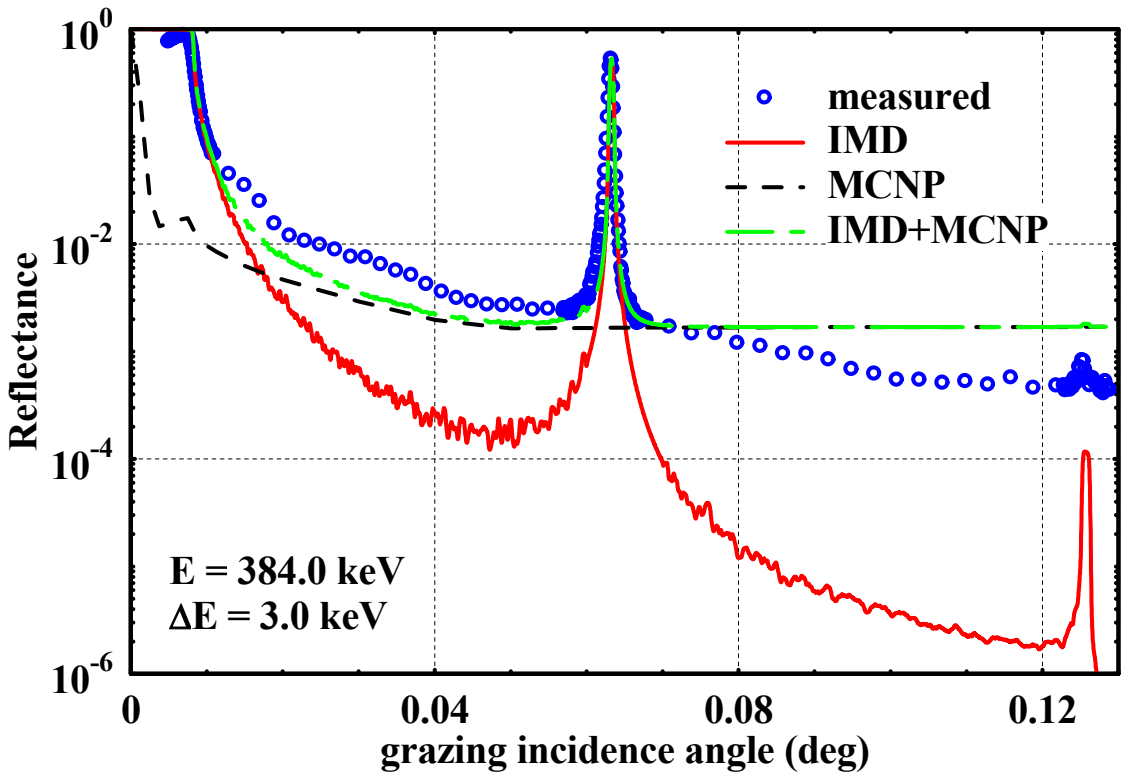
measured
IMD
MCNP
IMD+MCNP
E = 384.0 keV
ΔE = 3.0 keV
Reflectance
grazing incidence angle (deg)
10^0
10^-2
10^-4
10^-6
0
0.04
0.08
0.12

Fig. 3.

References

[1] P. Gorenstein, Opt. Eng. **51,** 011010 (2012).

[2] F. Berendse, S. M. Owens, P. J. Serlemitsos, J. Tueller, K.-W. Chan, Y. Soong, H. Krimm, W. H. Baumgartner, Y. Ogasaka, K. Tamura, T. Okajima, Y. Tawara, K. Yamashita, K. Misaki, and H. Kunieda, Appl. Opt. **42,** 1856 (2003).

[3] D. L. Windt, F. E. Christensen, W. W. Craig, C. Hailey, F. A. Harrison, M. Jimenez-Garate, R. Kalyanaraman, and P. H. Mao, J. Appl. Phys. **88,** 460 (2000).

[4] D. L. Windt, S. Donguy, C. J. Hailey, J. Koglin, V. Honkimaki, E. Ziegler, F. E. Christensen, H. Chen, F. A. Harrison, and W. W. Craig, Appl. Opt. **42,** 2415 (2003).

[5] Y. Ogasaka, T. Iwahara, T. Miyazawa, Y. Fukaya, N. Sasaki, K. Tamura, Y. Kanou, H. Kunieda, and K. Yamashita, Proc. SPIE **6688,** 66880S (2007).

[6] E. Spiller, *Soft X-Ray Optics* Ch. 7 (SPIE Optical Engineering Press, Bellingham, 1994).

[7] D. Habs, M. M. Günther, M. Jentschel, and W. Urban, Phys. Rev. Lett. **108**, 184802 (2012).

[8] C. P. Jensen, N. Brejnholt, S. Romaine, R. Bruni, F. E. Christensen, D. H. Lumb, and Z. Zhong, Proc. SPIE **7011,** 70111K–1 (2008).

[9] P. B. Mirkarimi, Opt. Eng. **38,** 1246 (1999).

[10] C. P. Jensen, K. K. Madsen, and F. E. Christensen, Exp. Astron. **20,** 93 (2005).

[11] M.D. Abad, M.A. Muñoz-Marquez, S. El Mrabet, A. Justo, and J.C. Sanchez-Lopez, Surf. Coat. Tech. **204,** 3490 (2010).

[12] D. L. Windt, Computers in Physics **12,** 360 (1998). Available at http://www.rxollc.com/idl/index.html.

[13] MCNP6 Initial MCNP6 Release Overview MCNP6 Beta 2, Los Alamos National Laboratory report LA-UR-11-07082.

[14] M. Born and E. Wolf, *Principles of Optics* (Cambridge Univ. Press, New York, 1980).

[15] M. Fernández-Perea, M. J. Pivovaroff, R. Soufli, J. Alameda, P. Mirkarimi, M.-A. Descalle, S. L. Baker, T. McCarville, K. Ziock, D. Hornback, S. Romaine, R. Bruni, Z. Zhong, V. Honkimäki, E. Ziegler, F. E. Christensen, and A. C. Jakobsen, Nucl. Instrum. Meth. A **710,** 114 (2013).

[16] C. T. Chantler, J. Phys. Chem. Ref. Data **24,** 71 (1995). Available on line at http://physics.nist.gov/ffast.

[17] C. T. Chantler, J. Phys. Chem. Ref. Data **29**, 597 (2000). Available on line at http://physics.nist.gov/ffast.

[18] R. Soufli, S. L. Baker, J. C. Robinson, E. M. Gullikson, T. J. McCarville, M. J. Pivovaroff, P. Stefan, S. P. Hau-Riege, and R. Bionta, Proc. SPIE **7361,** 73610U (2009).

[19] D. E. Cullen, J. H. Hubbell, and L. Kissel, EPDL97: The evaluated photon data library. Lawrence Livermore National Laboratory report UCRL-50400, vol. 6, rev. 5 (1997), available from the National Technical Information Service, U.S. Department of Commerce, 5285 Port Royal Road, Springfield, VA 22161.

[20] M. J. Pivovaroff, , T. Funk, W. C. Barber, B. D. Ramsey, and B. H. Hasegawa, Proc. SPIE **5923,** 59230B (2005).

[21] K.-H. Yoon, Y. M. Kwon, B.-J. Choi, H. H. Son, C. W. Ryu, K. S. Chon, S. H. Park, and S. K. Juhng, Invest. Radiol. **47,** 683 (2012).

[22] F. A. Harrison et al., [arXiv:1301.7307].

[23] T. Takahashi et al., Proc. SPIE **8443,** 84431Z (2012).

[24] Y. Seo, C M. Aparici, and B. H. Hasegawa, Sem. Nucl. Med. **38**, 177 (2008).

[25] G. Mariani, L. Bruselli, T. Kuwert, E. E. Kim, A. Flotats, O. Israel, M Dondi, and N.

Watanabe, Eur. J. Nucl. Med. Mol. Imaging **37**, 1959 (2010).

[26] S. Adak, R. Bhalla, K. K. Vijaya Raj, S. Mandal, R. Pickett, and S. K. Luthra, Radiochim. Acta **100**, 95 (2012).

[27] J.-P. Roques, E. Jouradin, L. Bassani, A. Bazzano, R. Belmont, A. J. Bird, E. Caroli, M. Chauvin., D. Clark, N. Gehrels, U. Goerlach, F. Harrisson, P. Laurent, J. Malzac, P. Medina, S. Paltani, J. Stephen, P. Ubertini, and J. Wilms, Exp. Astron. **34,** 489 (2012).

[28] R. Diehl, Rep. Prog. Phys. **76** 026301 (2013).

[29] E.-J. Buis, M. Beijersbergen, G.Vacanti, M. Bavdaz, and D. Lumb, Exp. Astron. **20,** 105 (2005).

[30] M. Aguilar, et al., Phys. Rev. Lett. **110**, 141102 (2013).

Figure captions

Fig. 1. Structure and morphology of WC/SiC coatings. (a) Multilayer design parameters of the four samples presented in this work. d is the multilayer period, with $d = d_{WC} + d_{SiC}$. d_{WC} and d_{SiC} are the individual WC and SiC layer thicknesses, respectively. N is the number of WC/SiC pairs and Γ_{WC} is the ratio of WC layer to period thickness ($\Gamma_{WC} = d_{WC}/d$). The first (bottom) layer deposited was a WC layer and the last (top) layer deposited was a SiC layer. (b) TEM image obtained on a 1.5 nm-period WC/SiC multilayer with $\Gamma_{WC} = 0.4$, deposited on an ultra-smooth, 525 μm-thick Si (100) wafer substrate. The thickness of the TEM sample in the direction perpendicular to the image plane is 100 nm. (c) LAXRD measurements at 8 keV, obtained in $\theta/2\theta$ geometry on a 2 nm-period WC/SiC multilayer with $\Gamma_{WC} = 0.8$.

Fig. 2. Experimental reflectance obtained at the ID15A beamline of the ESRF at a photon energy of 378.2 keV for samples with different period thickness (d). The crystal monochromator was set at an energy bandwidth of $\Delta E = 9.8$ keV. The 1st order Bragg peak is shown for each sample.

Fig. 3. Experimental reflectance values obtained at the ID15A beamline of the ESRF synchrotron at a photon energy of 384.0 keV for the 1.5 nm-period sample. The crystal monochromator detuning was set at an energy bandwidth of $\Delta E = 3.0$ keV. A shift of 0.95 mdeg was applied to the measured values to account for a small misalignment of the sample. The lines correspond to the IMD[12] wave model, the MCNP[13] particle model, and the additive combination of the two.